4.1. Introduction

It was observed from last few years, dielectric materials under perovskite oxides have been studied very widely with variation of temperature and frequency [Lee *et al*. (2014), Carpi *et al*. (2008), Yadava *et al*. (2016a)].The isovalent or heterovalent partial doping of metal ions having same or little different ionic size as compared to metal ions present at sites A and B of the perovskite oxides enhances its electrical properties due to increase in polarization or structural changes [Ul-ain *et al*. (2013)]. A well-known material, barium titanate shows excellent dielectric and ferroelectric properties with respect to temperature, frequency and electrical voltage [Weber *et al*. (2001), Moura *et al*. (2008)]. Such interesting properties of barium titanate are possible due to position of titanium ions at B site was not fixed, it will shift from its expected position which creates the polarity. The dielectric and ferroelectric properties increase on doping of any other transition metal at titanium site [Haertling (1999)]. The degree of distortion in structure of perovskites (ABO_3) is mainly due to the size of A and B ions. The Goldsmith tolerance factor $t = (r_A + r_O)/\sqrt{2} * (r_B + r_O)$ where r_A represents ionic radius of cation (Ba^{2+}, Ca^{2+}), r_B represents ionic radius of the 3rd row of transition metal ion and r_O is the radius of oxide ion. The value of tolerance factor (t) is responsible for structural distortion of the perovskite oxides [Moure *et al*. (2002)]. The doping of iron at B site of the perovskites will reduce dielectric constant drastically because of inhibition in the formation of barrier layers at grain boundary [Rai *et al*. (2011), Mu *et al*. (2010)]. The semiconducting grains and insulating grain boundaries are main cause of high dielectric permittivity of perovskite materials which follow IBLC mechanism [Ahmad and Yamada (2014)]. The transition metals doped perovskites having magnetic, ferroelectric and dielectric properties are highly useful for data storage media [Fiebig *et al*. (2002)] and memory device [Hill (2000)]. The high dielectric

constant and variable oxidation states of $Mn^{3+/4+}$ in hexagonal perovskites $Ba_4YMn_3O_{11.5-\delta}$ (BYMO) have temperature dependent ferroelectric properties [Yadava *et al*. (2016a), Kuang *et al*. (2012)]. The presence of face sharing or corner sharing by oxide linkage of MnO_6 and YO_6 octahedra in BYMO ceramic is responsible for its unique dielectric, ferroelectric and magnetic properties [Baibier *et al*. (2012)]. The effect on dielectric constant of copper doping at manganese site of hexagonal BYMO ceramic studied earlier [Barbier *et al*. (2013)]. In this chapter $Ba_4YMn_{3-x}Fe_xO_{11.5}$ (x = 0.05, 0.1, 0.2) ceramics was synthesized by chemical route and performed detailed structural studies by Rietveld refinement of XRD data, particle size analysis by TEM, SEM and AFM. The dielectric, ferroelectric and magnetic properties of all samples were carefully investigated with variation of parameters such as temperature, frequency, magnetic field and electric field.

4.2. Experimental

$Ba_4YMn_{3-x}Fe_xO_{11.5-\delta}$ (x = 0.05, 0.1 and 0.2) which were also noted as BYMFO-05, BYMFO-1 and BYMFO-2 respectively, and all these compositions also represented by BYMFO, synthesized by chemical route in which metal ions are taken in form of their nitrates/acetates salts. The chemicals used are of analytical grade and are used without further purification $Ba(NO)_2.6H_2O$ (99 % Merck India), $Y(NO)_3.6H_2O$ (99.8 % Merck India), $Mn(ac)_2.2H_2O$ (99.99 % Sigma-Aldrich India), and $Fe(NO)_3.H_2O$ (98 % Merck India). The stoichiometric amount of all metal nitrates were taken and dissolved in double distilled water separately and then mixed in a beaker. The calculated amount of glycine per equivalent of metal ions was taken and dissolved in double distilled water which was added in the solution. The reaction mixture was heated on hot plate with continuous stirring at 70 – 80 ^{0}C to evaporate

water. After removal of water a gel was formed which burns with flame on further heating and obtained a fluffy mass. The resulting material was grounded with agate and mortar to make it fine powder. Calcination and grinding of material was done at 500 and 800 ^{0}C for 6 and 8 h respectively. Calcined powder at 800 ^{0}C was used to make cylindrical pellets (10mm×1mm) using polyvinyl alcohol as binder. Pellets were heated at 500 ^{0}C for 4 h to remove PVA binder. Finely pellets were sintered at 1100 ^{0}C for 12 h. The pellets were polished with emery paper to make its surfaces smooth and silver paint was coated on both the sides of circular disc for dielectric and ferroelectric measurement. The synthesized material was characterized by powder XRD (Rigaku miniflex 600 Japan) at scan rate of 1°/min from 2θ value 20-80^0 keeping step size 0.02 constant, HR-SEM and EDX mapping (FEI NOVA NANO SEM 450), and TEM ((TECHNAI G^2 TWIN)). DC magnetization of materials were performed by MPMS (SQUID Magnetometer Quantum design), Temperature and frequency dependence dielectric properties measured by PSM1735 NumetriQ (U.K), Ferroelectric properties and its temperature dependence remanent polarization was measured by (PE loop tracer- Marine India).

4.3. Result and discussion

4.3.1. Characterization

Figure 4.1 shows the Rietveld refinement of X-ray diffraction pattern of $Ba_4YMn_{2.95}Fe_{0.05}O_{11.5-\delta}$ ceramics sintered at 1100 ^{0}C for 12 h which confirms the hexagonal structure with space group $R\bar{3}m$. The observed structural and lattice parameters of $Ba_4YMn_{3-x}Fe_xO_{11.5-\delta}$ (x = 0.05, 0.1, 0.2) are shown in Table 4.1 and 4.2.

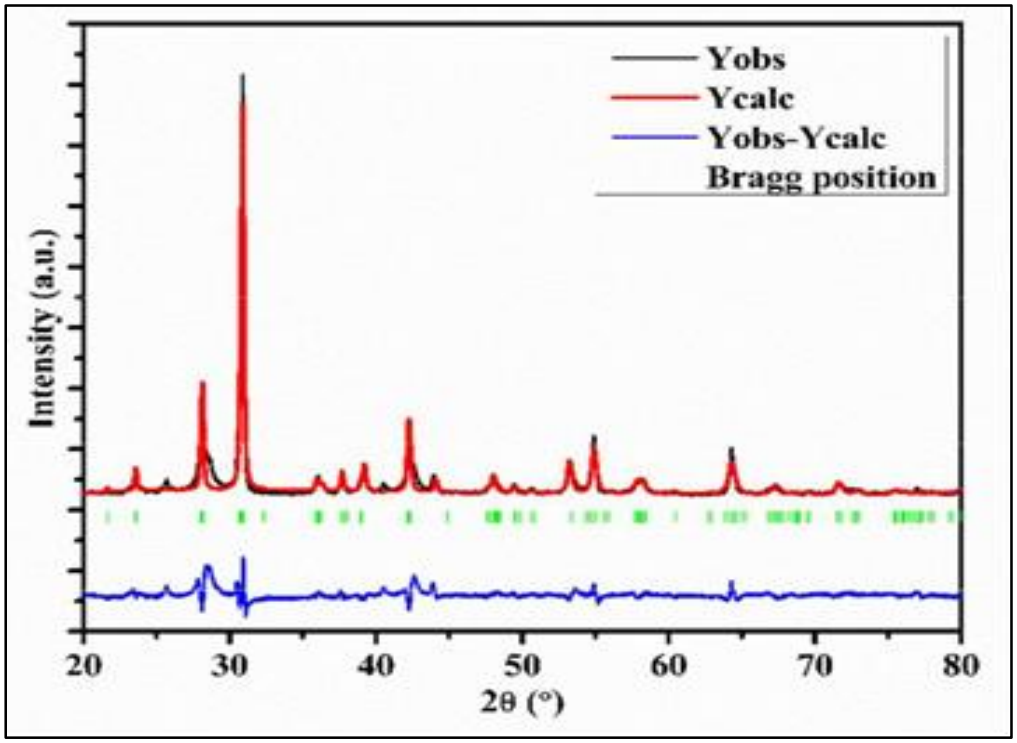

Figure 4.1 Rietveld refinement of XRD data $Ba_4YMn_{2.95}Fe_{0.05}O_{11.5-\delta}$ hexagonal perovskite oxide having space group $R\bar{3}m$

Table 4.1 Refined structural parameters obtained by Rietveld refinement of $Ba_4YMn_{3-x}Fe_xO_{11.5-\delta}$ (x = 0.05, 0.1, 0.2) ceramic

Atom	**X** **(x = 0.05, 0.1, 0.2)**	**Y** **(x = 0.05, 0.1, 0.2)**	**Z** **(x = 0.05, 0.1, 0.2)**
Ba1	2/3, 2/3, 2/3	1/3, 1/3, 1/3	0.06611, 0.06621, 0.06531
Ba2	0, 0, 0	0, 0, 0	0.14531, 0.14542, 0.14532
Y	0, 0, 0	0, 0, 0	0, 0, 0
Mn1/Fe1	1/3, 1/3, 1/3	2/3, 2/3, 2/3	0.08149, 0.08142, 0.08148
Mn2/Fe2	1/3, 1/3, 1/3	2/3, 2/3, 2/3	0.1666, 0.1666, 0.1666
O1	0.7156, 0.7244, 0.7214	0.3968, 0.3743, 0.3701	0.1126, 0.1325, 0.1314
O2	0.2255, 0.3141, 0.2253	0.4516, 0.5423, 0.4431	0.3277, 0.2453, 0.3082

Table 4.2 The values of lattice parameter, χ^2 and space group of $Ba_4YMn_{3-x}Fe_xO_{11.5-\delta}$ (x = 0.05, 0.1, 0.2) ceramics obtained by Rietveld refinement

$Ba_4YMn_{3-x}Fe_xO_{11.5-\delta}$	a = b (Å)	c (Å)	χ^2	Space group
x = 0.05	5.7895	28.6405	4.56	$R\bar{3}m$
x = 0.10	5.7758	28.6402	4.58	$R\bar{3}m$
x = 0.20	5.7804	28.6314	4.43	$R\bar{3}m$

The structural parameter values are almost same as that of copper doped BYMO ceramic which was reported earlier [Barbier *et al*. (2013)]. The X-ray diffraction patterns of BYMFO-05, BYMFO-1 and BYMFO-2 are shown in Figure 4.2 indicating similar peak positions which confirm the hexagonal phase in all compositions. All peaks were indexed according to JCPDS file no (26-0166).

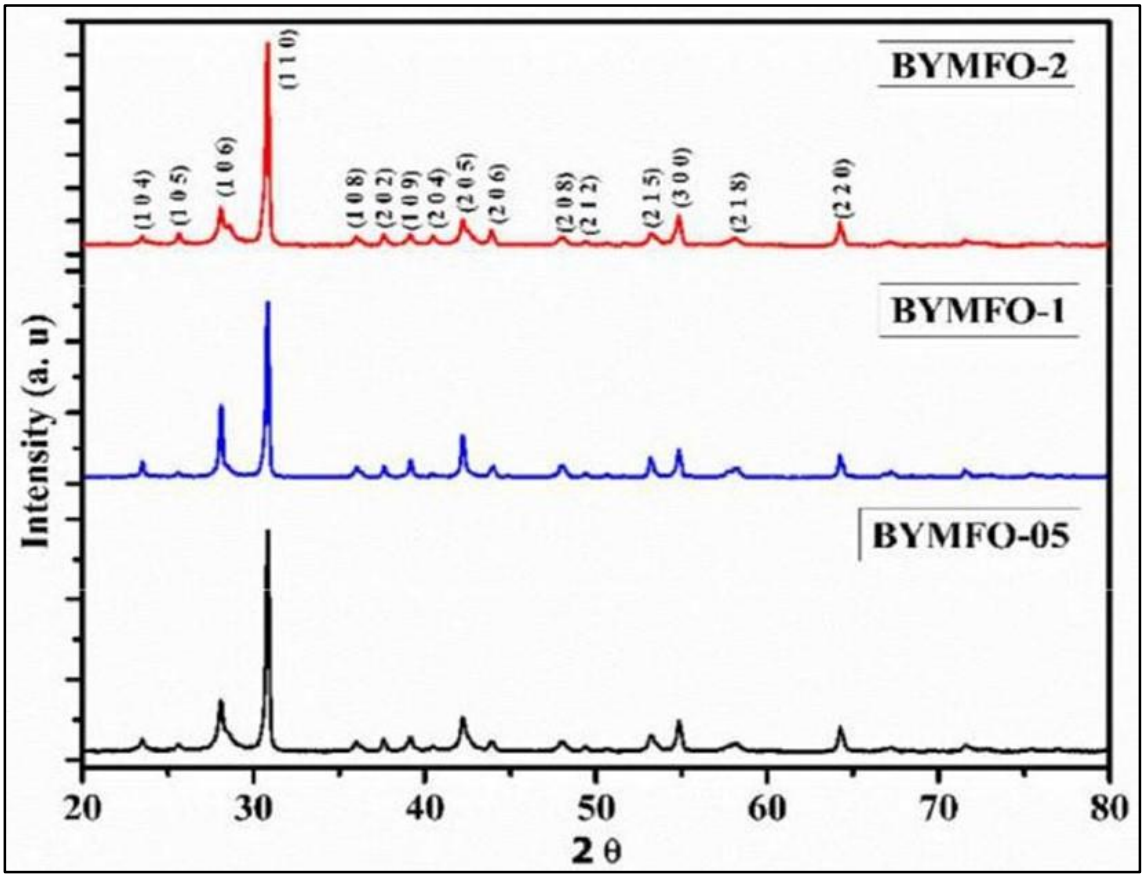

Figure 4.2 X-ray diffraction patterns of BYMFO-05, BYMFO-1 and BYMFO-2 sintered at 1100 ^{0}C for 12 h

The surface morphology of sintered sample of BYMFO were studied firstly with SEM. For SEM images, the gold coated surfaces of BYMFO-05, BYMFO-1 and BYMFO-2 were used and observed morphology shown in Figure 4.3 (a, b and c). The figures indicate the distribution of small and large grains which are separated by grain boundary. The calculated grain size was found to be 350 nm, 300 nm and ~90 nm for BYMFO-0.05, BYMFO-1 and BYMFO-2 ceramics respectively. The formation of hexagonal faces is clearly seen (Fig. 4.3 (c)) which support the presence of hexagonal structure of BYMFO ceramics. Figure 4.3 (d) indicates the elemental mapping of BYMFO-2, in which each element is shown by specific colors, indicates

homogeneous and heterogeneous distribution of elements at different areas of the sample. The elemental percentages confirm the presence of Ba, Y, Mn, Fe and O in BYMFO-2 ceramic.

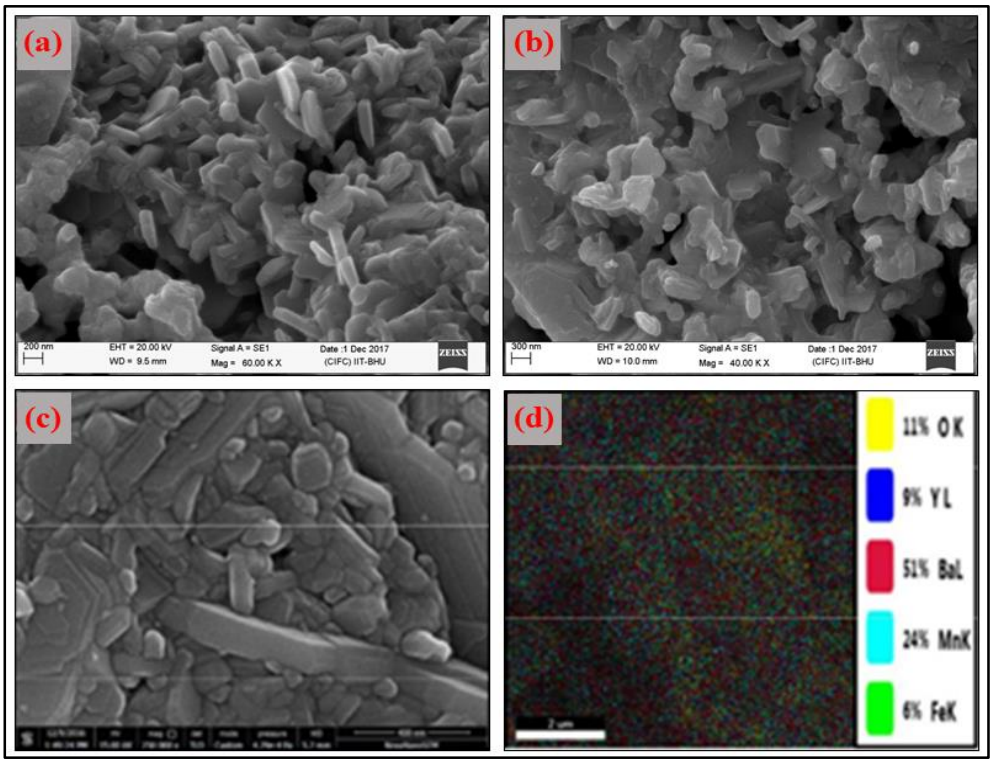

Figure 4.3 Surface morphology of **(a)** BYMFO-05, **(b)** BYMFO-1 **(c)** BYMFO-2 ceramics obtained by SEM and **(d)** elemental mapping of BYMFO-2 ceramic obtained by EDX

Bright field TEM images of BYMFO-05, BYMFO-1 and BYMFO-2 ceramics are shown in Figures 4.4 (a, b and c). The figure clearly shows the formation of nano-sized particles in all the synthesized BYMFO ceramics. It also shows that the particle size decreases with increasing iron concentration of Fe-doped BYMO ceramic. Figure 4.4 (c), indicates majority of particles are of similar size. The calculated average particles size was found to be 40 nm, 23 nm and 6 nm for BYMFO-05, BYMFO-1 and BYMFO-2 respectively. The grain size observed from

SEM is larger than particle sizes observed by TEM. Grains are generally greater than particles due to, it is formed by the combination of few particles.

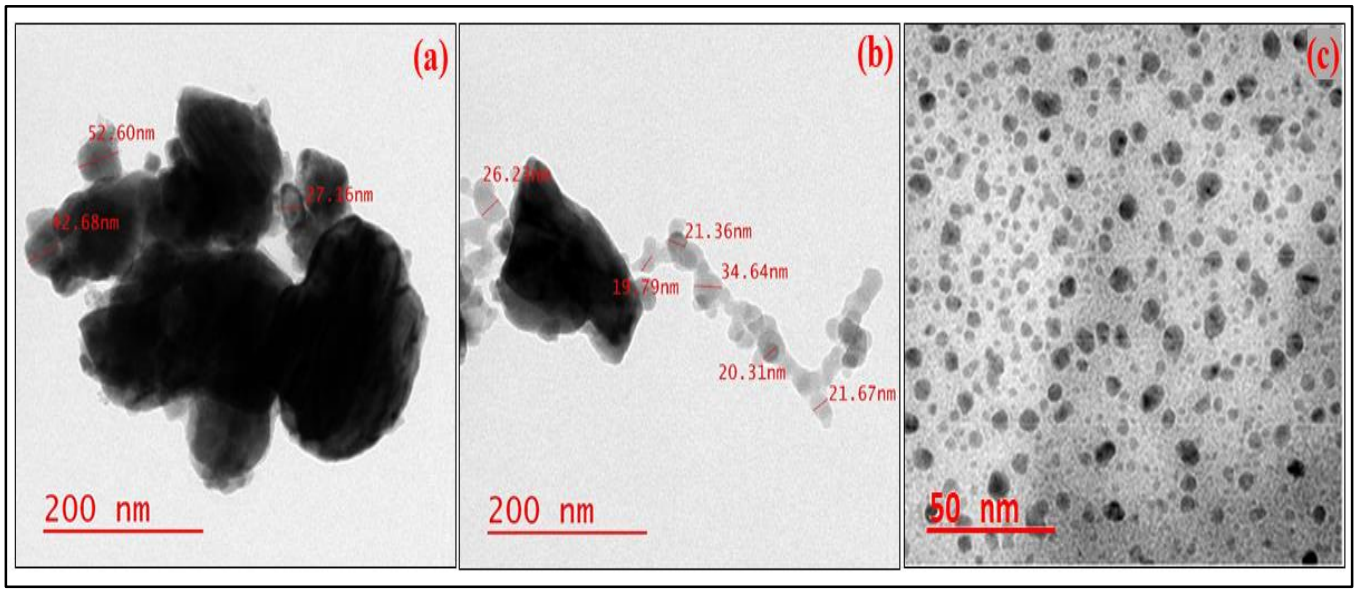

Figure 4.4 TEM images of **(a)** BYMFO-05 **(b)** BYMFO-1 and **(c)** BYMFO-2 ceramics sintered at 1100 ^{0}C for 12 h

4.3.2. Dielectric properties

Figure 4.5 shows room temperature dielectric constant with frequency of BYMFO-05, BYMFO-1 and BYMFO-2 from 100 Hz –5 MHz. As iron concentration increase dielectric constant decrease very rapidly from 872 to 54 at 100 Hz. The inverse behavior of dielectric constant with frequency due to alignment of polarization direction on changing alternating field frequency [Ravinder and Kumar. (2001)].

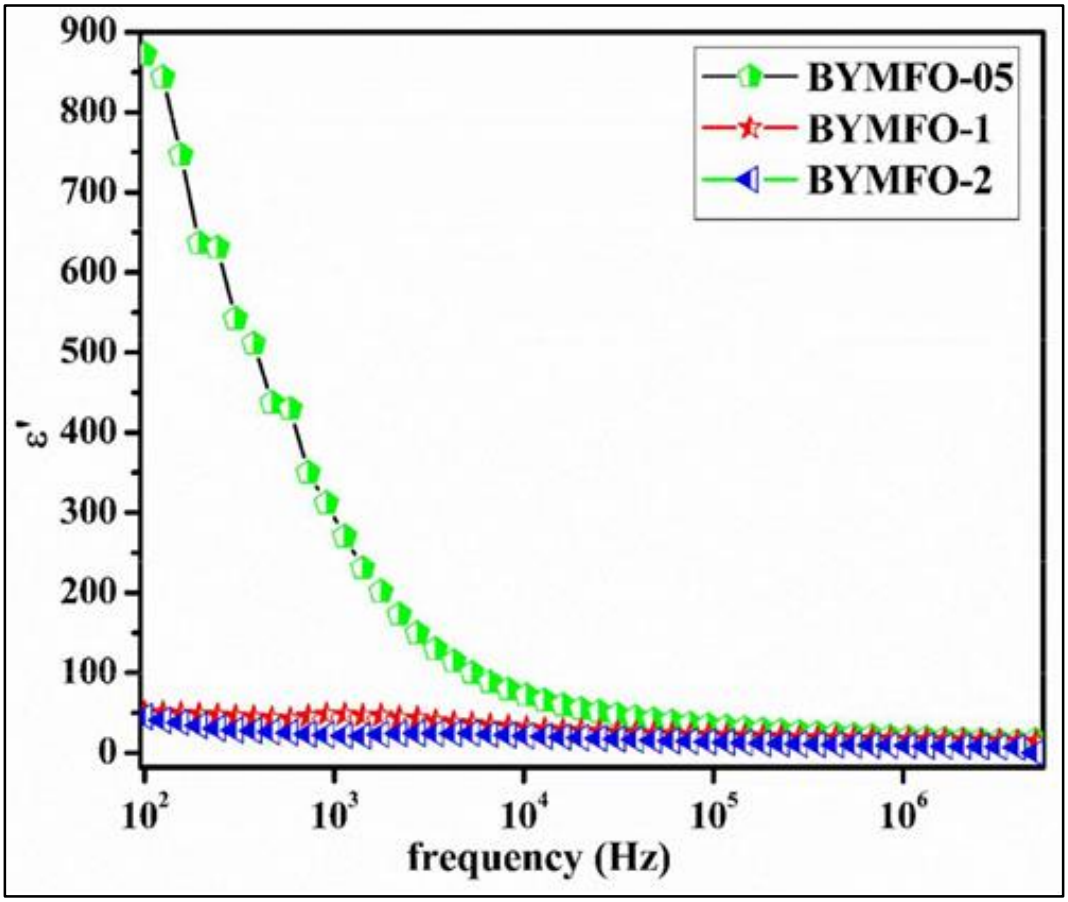

Figure 4.5 Frequency dependent dielectric constants of BYMFO-05, BYMFO-1 and BYMFO-2 ceramics at 300 K

At higher frequency the movement of charge is not keep up with frequency which ceases the contribution of polarization towards dielectrics [Rajwali and Ming (2015)]. The dielectric constant calculated by the following equation (4.1) [Puli *et al*. (2016), Prakash and Verma (2007)].

$$\varepsilon_r = \frac{cd}{\varepsilon_0 A} \qquad (4.1)$$

where ε_o (8.85×10^{-12} $m^{-3}kg^{-1}s^4A^2$) is the permittivity of free space, C, d, and A are capacitance, width and area respectively of the cylindrical pellet. Figure 4.6 shows variation of dielectric

loss with frequency. It is clear from the figure that the dielectric loss decreases with frequency due to energy dissipate during polarization changes its direction in applied electric field frequency such interaction between dielectric polarization with field results heating. The temperature dependence dielectric constant of BYMFO-05, BYMFO-1 and BYMFO-2 demonstrate in Figure 4.7 at 1 kHz of frequency.

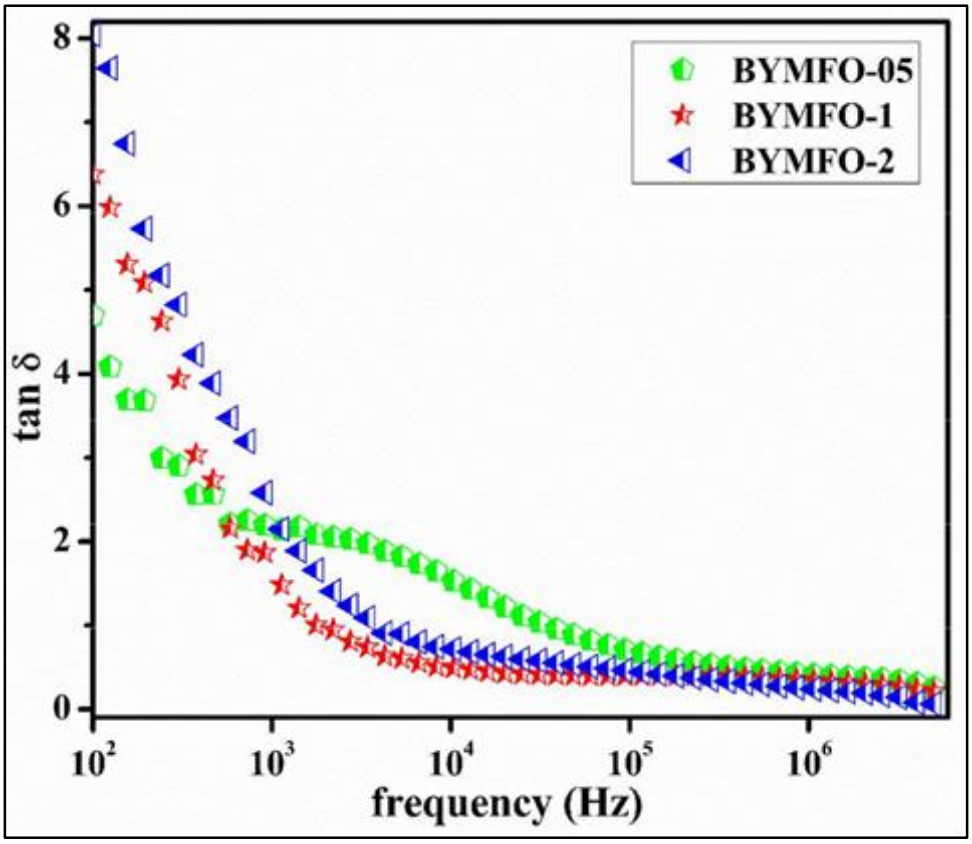

Figure 4.6 Frequency dependent dielectric loss of BYMFO-05, BYMFO-1 and BYMFO-2 ceramics at 300 K

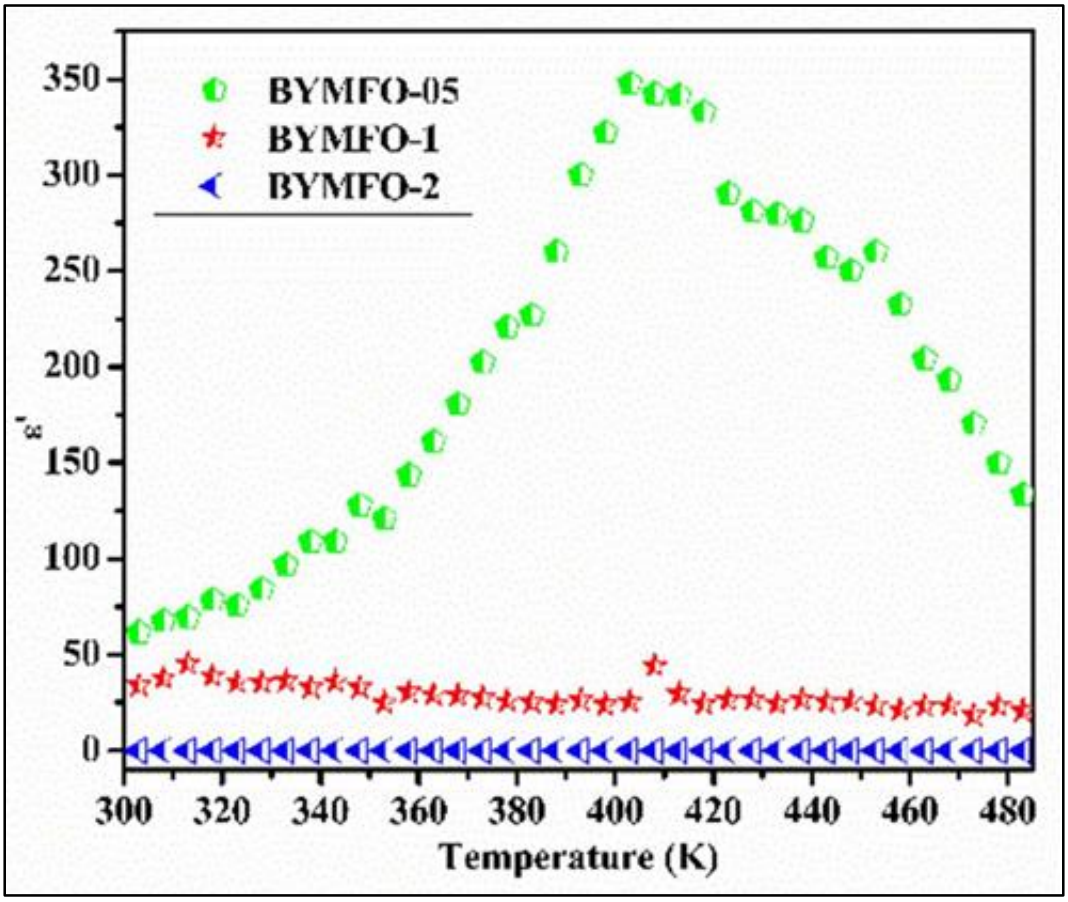

Figure 4.7 Dielectric constant Vs temperature plot of BYMFO-05, BYMFO-1 and BYMFO-2 ceramics at 1 kHz, 300 K

Debye type dielectric relaxation was observed only in case of BYMFO-05 which may be due to surface layer interfacial polarization [Zheng *et al*. (2016)] whereas temperature independent permittivity observed in case of BYMFO-1 and BYMFO-2. This temperature dependent dielectric constant in BYMFO-05 and temperature independent dielectric constant in BYMFO-1, BYMFO-2 indicates ferroelectric to paraelectric transitions. The curie temperature of BYMFO-05 was calculated and found to be 410 K. The impedance plane plot (Z' vs Z") of BYMFO-05, BYMFO-1 and BYMFO-2 were shown in Figure 4.8. In the case of BYMFO-05

two semicircular arc were observed which confirms the presence of semiconducting grains and insulating grain boundary, but only one semicircular arc corresponding to grain boundary was observed for BYMFO-1 and BYMFO-2 ceramics.

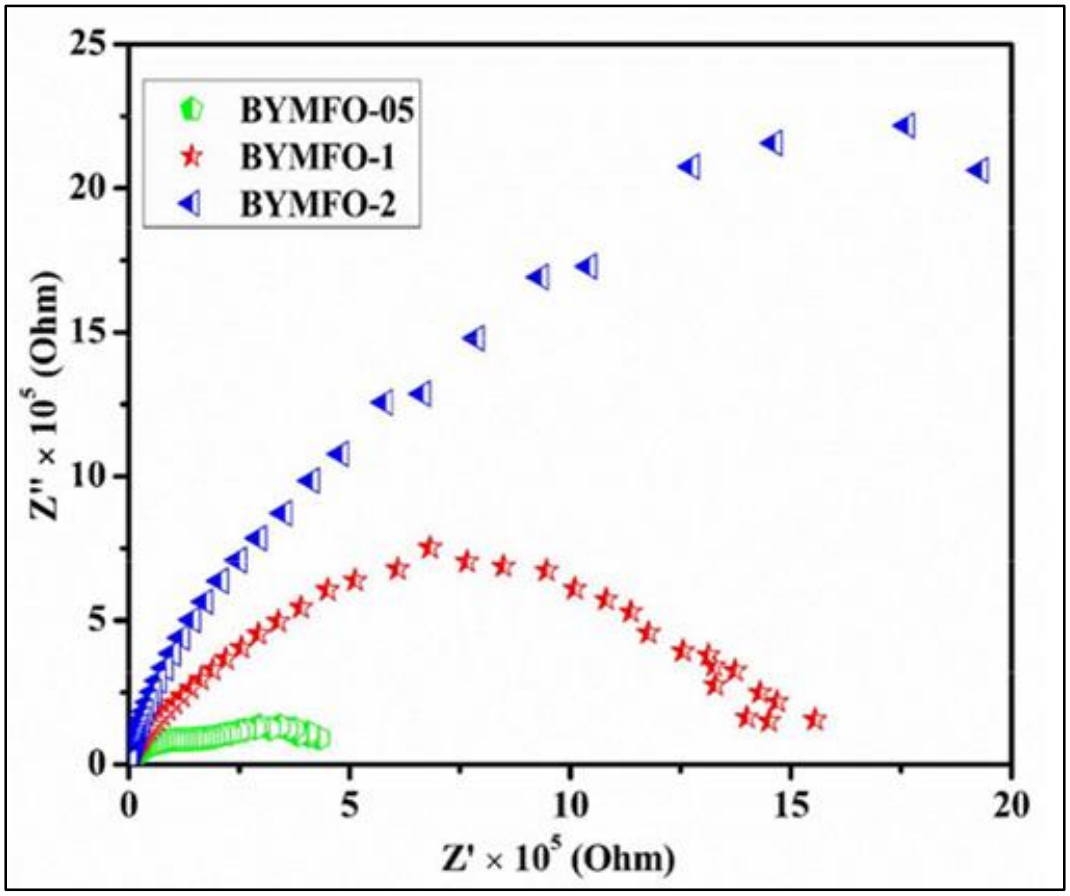

Figure 4.8 Impedance plane plot (Z" Vs Z') of BYMFO-05, BYMFO-1 and BYMFO-2 ceramics at 300 K

The presence of single semicircular arc is due to decrease of resistance on increasing iron concentration. Absence of grain contribution is the responsible factor for low dielectric constant of BYMFO-1 and BYMFO-2.

4.3.3. Magnetic and Ferroelectric properties

The temperature dependent DC magnetization was measured at 2000 Oe for all the iron doped samples. The magnetic hysteresis loop of BYMFO-05, BYMFO-1 and BYMFO-2 ceramics are shown in Figure 4.9, 4.10 and 4.11 respectively.

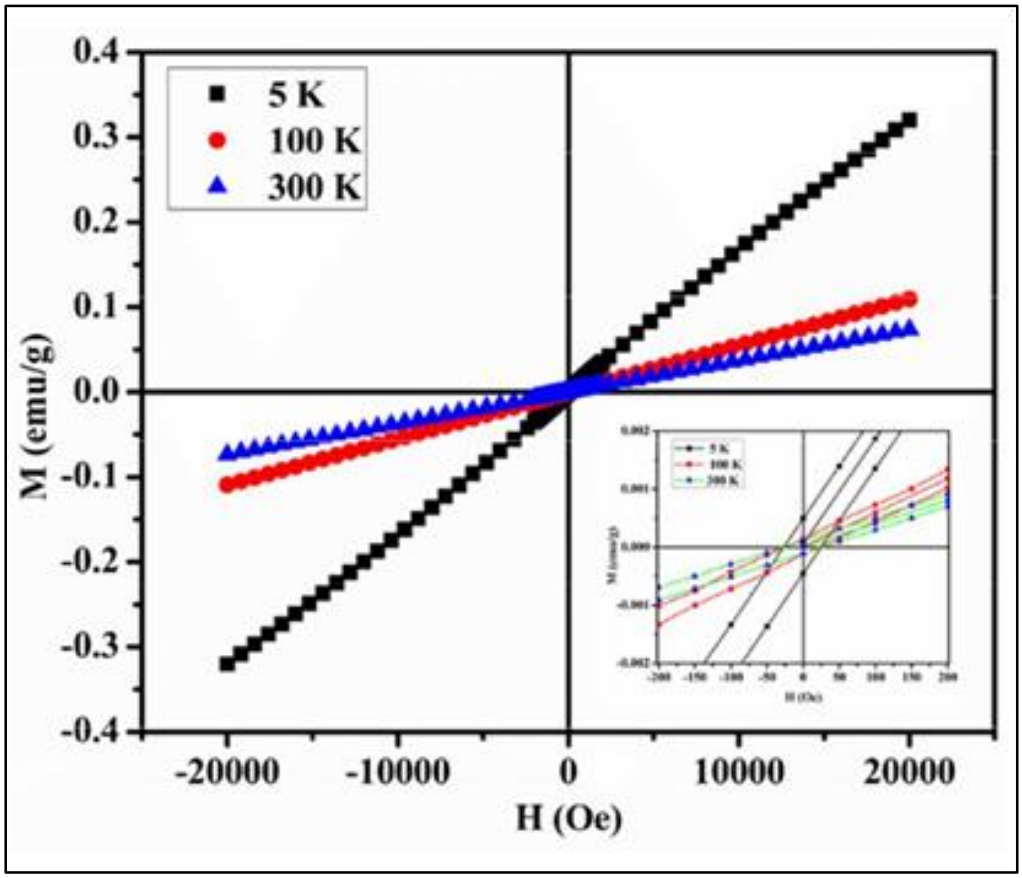

Figure 4.9 M-H hysteresis of BYMFO-05 at temperature of 5 K, 100 K and 300 K, whereas inset shows temperature dependent remanent magnetization

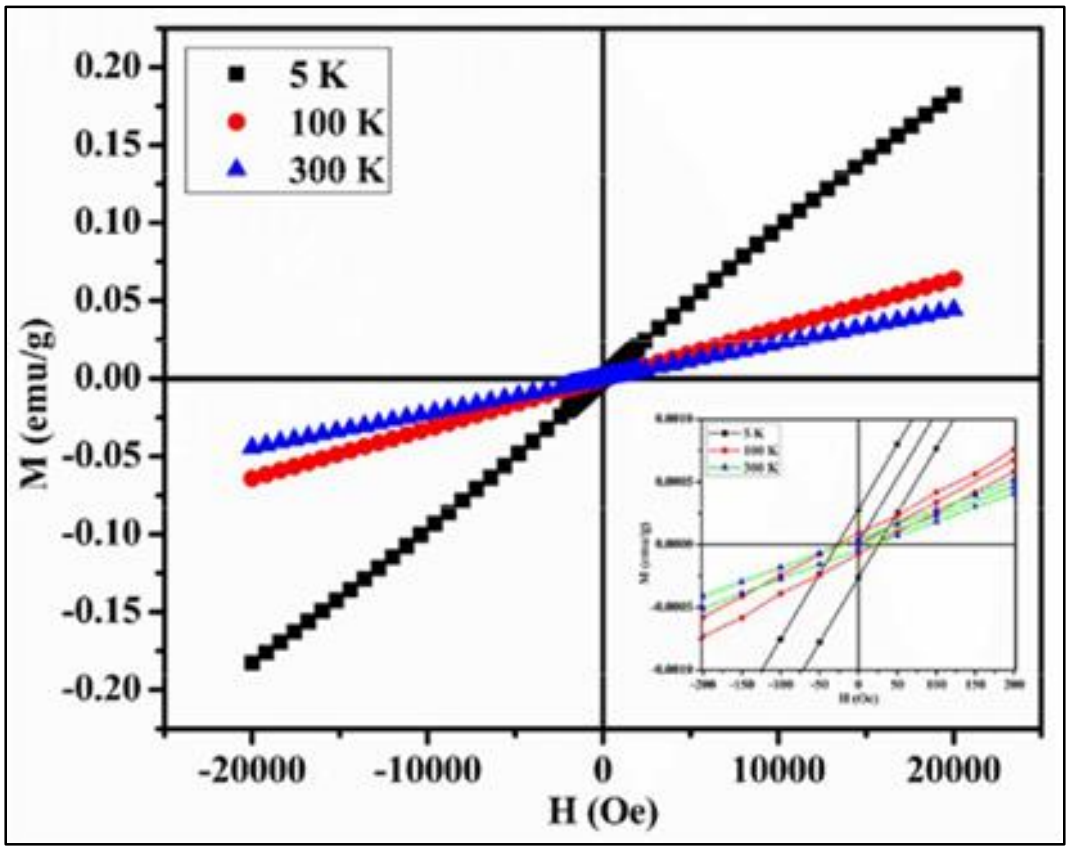

Figure 4.10 M-H hysteresis of BYMFO-1 at temperature of 5 K, 100 K and 300 K. The inset shows temperature dependent remanent magnetization

For all the above mentioned samples on increasing temperature weak ferromagnetic behavior convert towards paramagnetic character because of remanent magnetization increase with decrease of temperature due to disordering of magnetic domains [Agrinskaya *et al*. (2016)].

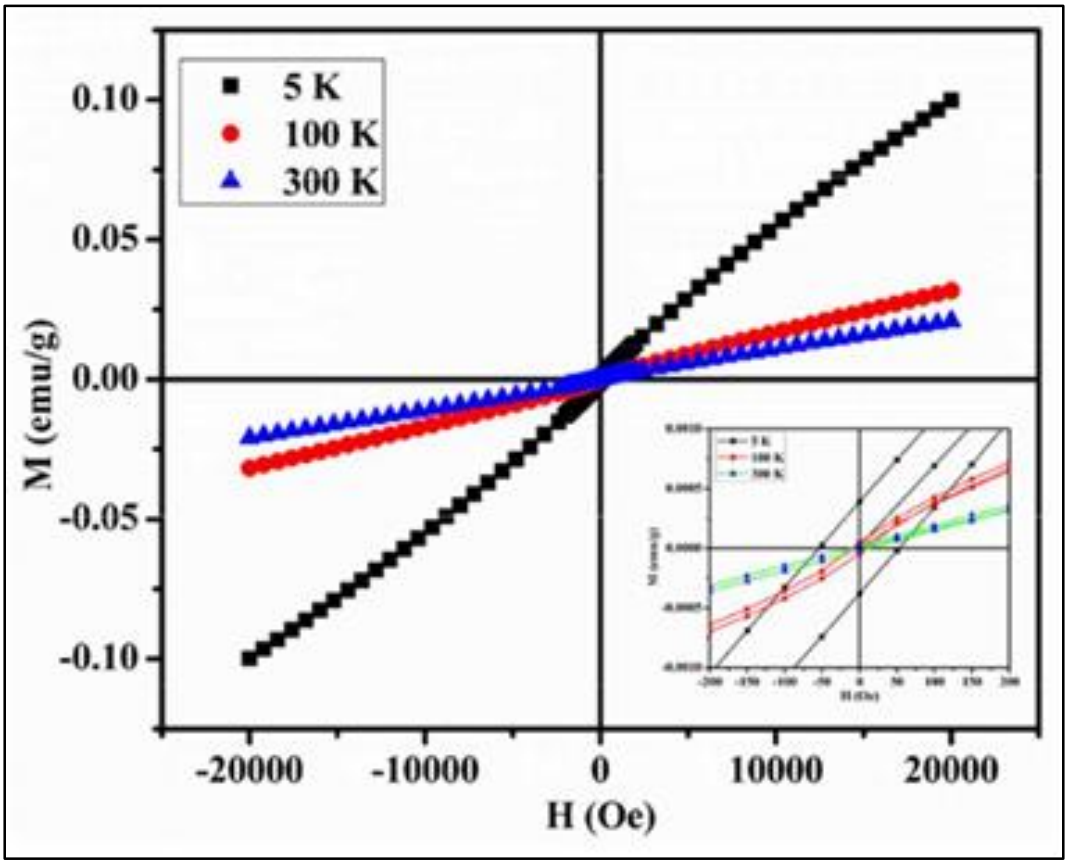

Figure 4.11 M-H hysteresis of BYMFO-2 at temperature of 5 K, 100 K and 300 K, whereas inset shows temperature dependent remanent magnetization

As iron concentration increase remanent magnetization at particular temperature decrease due to iron Fe^{3+} is paramagnetic. As the amount of iron increase super-exchange (SE) interaction between neighboring Fe^{3+} ions were anti-ferromagneticaly coupled through oxide linkage. As a result, enhanced super-exchange interaction $Fe^{3+}(d^5)–O^{2-}–Fe^{3+}(d^5)$ decrease the ferromagnetic coupling, resulting decrement in ferromagnetic moment [Babu *et al*. (2015)]. The corresponding values of remanent magnetization and coercive magnetic fields are shown in Table 4.3.

Table. 4.3 Remanent magnetization and coercivity of BYMFO-05, BYMFO-1 and BYMFO-2 at certain temperature

Temperature	**BYMFO-05**		**BYMFO-01**		**BYMFO-02**	
	Mr (emu/g)	**Ec (Oe)**	**Mr (emu/g)**	**EcOe)**	**Mr (emu/g)**	**Ec (Oe)**
5 K	4.95×10^{-4}	24.63	2.78×10^{-4}	27.34	3.89×10^{-4}	49.75
100 K	1.49×10^{-4}	24.63	8.97×10^{-5}	27.34	5.08×10^{-5}	10.33
300 K	1.14×10^{-4}	24.63	4.18×10^{-5}	27.34	2.12×10^{-5}	10.33

The temperature dependent magnetization, zero-field-cooled (ZFC) and field-cooled (FC) measurement was performed on BYMFO-2 at the fixed magnetic field of 1 Tesla as shown in Figure 4.12.

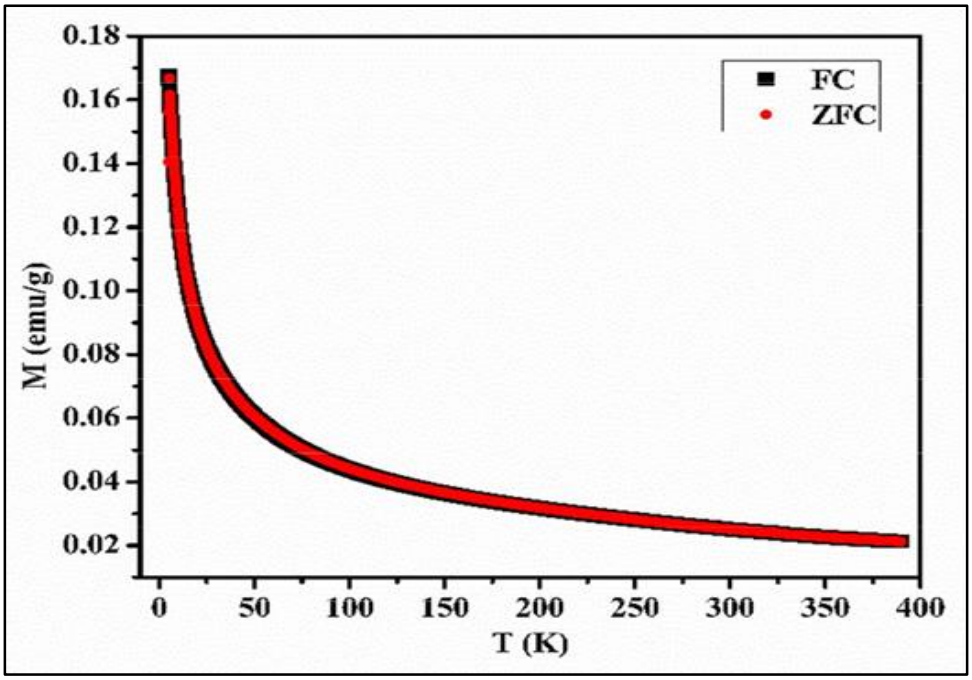

Figure 4.12 The temperature dependent FC and ZFC magnetization of BYMFO-2 at 1T of applied field

The both zero field and field cooled curves are completely coinciding through all temperature range and there is no blocking temperature observed. This indicates the complete super para-magnetic behavior of material.

Figure 4.13 shows P-E hysteresis loop of BYMFO-05, BYMFO-1 and BYMFO-2 nanoparticles measured at room temperature. The remanent polarization of BYMFO-05, BYMFO-1 and BYMFO-2 were found to be 0.925, 0.571 and 0.375 μC/cm^2 respectively.

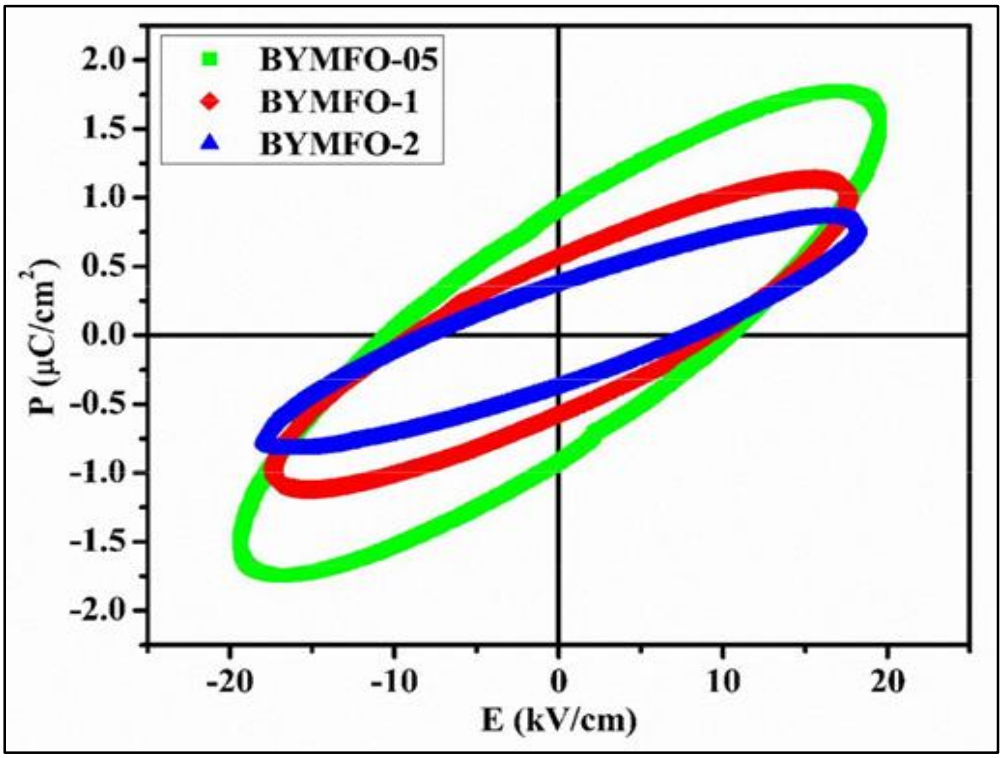

Figure 4.13 PE hysteresis loop of BYMFO-05, BYMFO-1 and BYMFO-2 ceramics at 300 K

The observe values of remanent polarization is very low this can be explained by iron reduces off center effect of MnO_6 octahedra and presence of oxygen vacancy in Fe^{3+} doped BYMO ceramic. The saturation polarization is not observed in all composition due to lossy capacitor nature of material [Stewart *et al.* (1999), Dutta *et al*. (2016), Das and Mandal (2011)]

4.4. Conclusion

All composition of $Ba_4YMn_{3-x}Fe_xO_{11.5-\delta}$ (x = 0.05, 0.1, 0.2) samples were successfully synthesized by chemical route at relatively low sintering temperature. The lattice parameter and atomic positions observed by Rietveld refinement confirms the Hexagonal structure of material having space group $R\bar{3}m$. High resolution scanning electron microscopy revels the formation of hexagonal crystal and the elemental mapping substantiate the compositional purity of the BYMFO ceramic. The remanent magnetization and remanent polarization increases with decrease of temperature. The dielectric constant of BYMFO ceramic decreases with increasing iron concentration in the ceramic. The inverse behavior of dielectric constant with frequency due to alignment of polarization direction on changing alternating field frequency.